

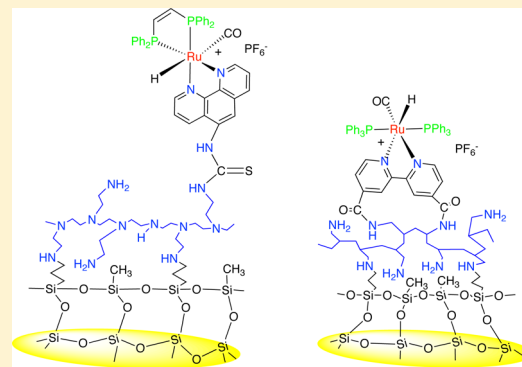
## Surface-Bound Ruthenium Diimine Organometallic Complexes: Excited-State Properties

Geoffrey Abbott, Robert Brooks, Edward Rosenberg,\* Michelle Terwilliger, J. B. Alexander Ross,\* and Ogar O. L. Ichire

Department of Chemistry & Biochemistry, University of Montana, Missoula, Montana 59812, United States

### S Supporting Information

**ABSTRACT:** Ruthenium complexes of the general formula  $[\text{Ru}(\text{CO})(\text{H})(\text{L}_2)(\text{L}'_2)][\text{PF}_6]$  ( $\text{L}_2 = \text{trans}-2\text{PPh}_3$ ,  $\text{L}' = \eta^2\text{-4,4'-dicarboxybipyridine}$  (1);  $\text{L}_2 = \text{trans}-2\text{Ph}_2\text{PCH}_2\text{CH}_2\text{COOH}$ ,  $\text{L}'_2 = \text{bipyridine}$  (2);  $\text{L}_2 = \text{Ph}_2\text{PCHCHPPh}_2$ ,  $\text{L}' = \eta^2\text{-5-amino-1,10-phenanthroline}$  (3);  $\text{L}_2 = \text{trans}-2\text{PPh}_3$ ,  $\text{L}'_2 = \eta^2\text{-4-carboxaldehyde-4'-methylbipyridine}$  (4)) have been shown to have longer emission lifetimes and higher quantum yields in solution compared with more symmetrical molecules such as  $[\text{Ru}(\text{bpy})_3][\text{Cl}]_2$ . Compound 4 is obtained as a mixture with the corresponding acetal, 4'. These less symmetrical complexes have been covalently immobilized on the surface of silica polyamine composites, and their photophysical properties have been studied. The surface-bound complexes have been characterized by solid-state CPMAS  $^{13}\text{C}$ ,  $^{31}\text{P}$ , and  $^{29}\text{Si}$  NMR, UV-vis, and FT-IR spectroscopies. Excited-state lifetime studies revealed that, in general, the lifetimes of the immobilized complexes are 1.4 to 8 times longer than in solution and are dependent on particle size (300–500  $\mu\text{m}$  versus 10–20 nm average diameter silica gels), polymer structure (linear poly(allylamine) versus branched poly(ethylenimine)), and the type of surface tether. One exception to this trend is the previously reported complex  $[\text{Ru}(\text{bpy})_2(\text{5-amino-1,10-phenanthroline})][\text{PF}_6]_2$  (5), where only a slight increase in lifetime is observed. Only minor changes in emission wavelength are observed for all the complexes. This opens up the possibility for enhanced heterogeneous electron transfer in photocatalytic reactions.



## INTRODUCTION

Surface and materials chemistry is becoming an increasingly studied field as the industrial and research sectors look into creating new materials that are useful in the areas of separations, catalysis, and sensors.<sup>1–6</sup> Knowledge of how binding a molecule to a surface affects different molecular properties is the key to being able to design and control the features needed for individual materials applications.<sup>7</sup>

One of the most promising opportunities for surface chemistry in both industry and academic research is the development of heterogeneous catalysts based on currently well-known homogeneous catalysts.<sup>2–6</sup> Any catalyst that can be bound to a surface and can maintain its ability to catalyze a reaction leads to an increase in efficiency, as time would no longer have to be spent separating catalyst from the products. Surface immobilization could also result in longer lasting catalysts, as the increased stability of a surface could protect the catalyst from degrading as quickly as it would in solution by intermolecular reactions. On the other hand, by placing the catalyst on a surface, access to reactants is hindered and the electron distribution could be affected by the surface in a deleterious way. Understanding what factors affect the surface-bound molecule and its electronic states is important in both designing the surfaces to bind catalysts and designing analogues

of these catalysts that can take advantage of certain surface features.

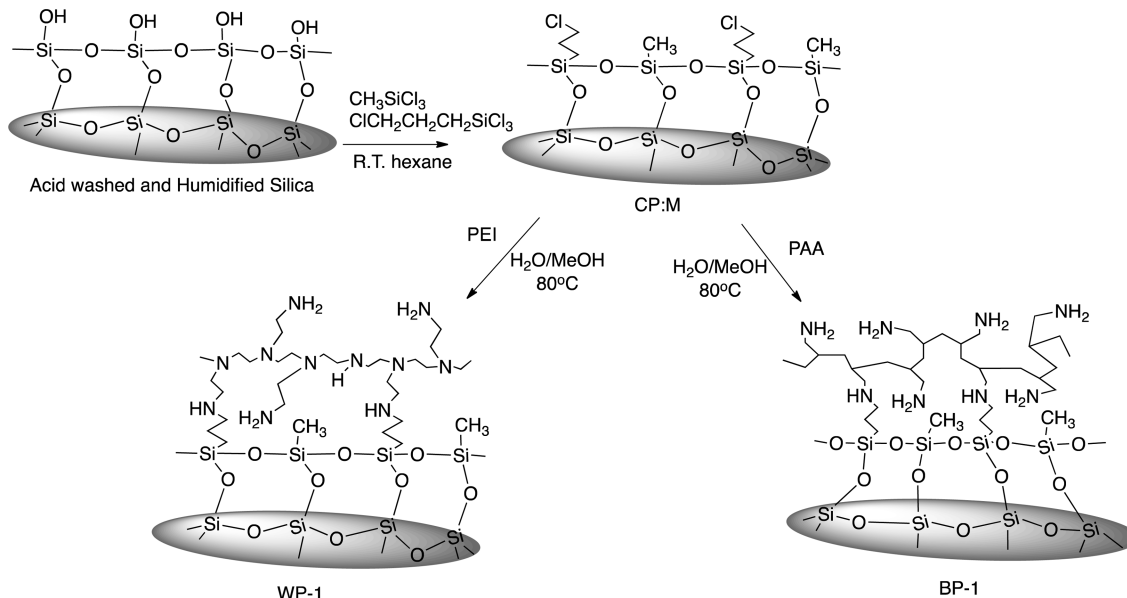
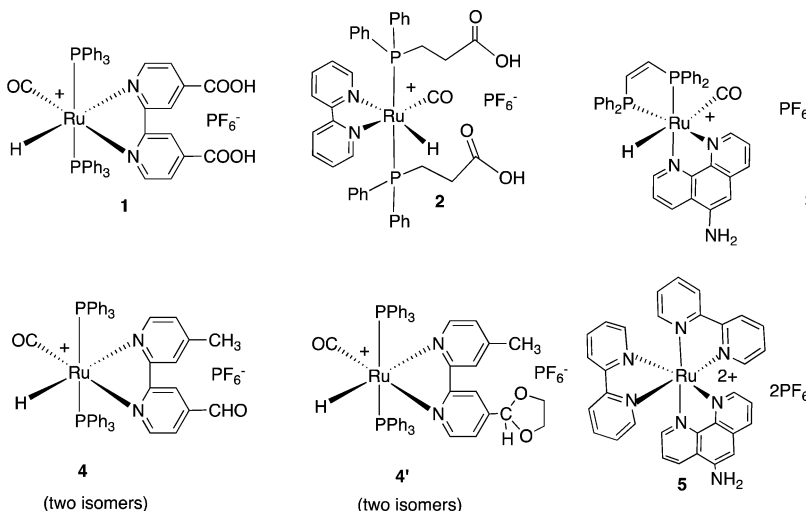
Amorphous silica gels are a common platform for surface chemistry, as they are readily available and their surfaces are easily modified through silanization chemistry.<sup>8–18</sup> We have previously reported that modification of silanized silica gels with a range of polyamines results in materials that selectively bind a wide range of metal ions after modification with metal-selective chelator ligands (Scheme 1).<sup>8–10</sup>

These silica polyamine composites (SPCs) have also been shown to act as hydrogenation catalysts after adsorption of late transition-metal salts.<sup>3</sup> Related studies have also shown that organometallic complexes covalently bound to a silica particle through a linker can be used as catalysts for various organic reactions.<sup>19</sup> Recently, luminescent Ru complexes have been covalently bound to silicon and silica nanoparticles for potential use as photo-optical devices.<sup>20,21</sup>

We report here the immobilization of the series of complexes  $[\text{Ru}(\text{CO})(\text{H})(\text{L}_2)(\text{L}'_2)][\text{PF}_6]$  ( $\text{L}_2 = \text{trans}-2\text{PPh}_3$ ,  $\text{L}' = \eta^2\text{-4,4'-dicarboxybipyridine}$  (1);  $\text{L}_2 = \text{trans}-2\text{Ph}_2\text{PCH}_2\text{CH}_2\text{COOH}$ ,  $\text{L}'_2 = \text{bipyridine}$  (2);  $\text{L}_2 = \text{Ph}_2\text{PCHCHPPh}_2$ ,  $\text{L}' = \eta^2\text{-5-amino-1,10-$

Received: November 26, 2013

Published: May 8, 2014

**Scheme 1.** Synthesis of Silica Polyamine Composites**Chart 1.** Structures of the Ruthenium Complexes Studied

phenanthroline (**3**);  $L_2 = \text{trans-}2\text{PPh}_3$ ,  $L'_2 = \eta^2\text{-4-carboxaldehyde-4'}\text{-methylbipyridine}$  (**4**)) on the SPC surface (Chart 1).

These complexes have previously been shown to have long excited-state lifetimes and higher quantum yields than the traditional tris-diimine ruthenium complexes such as  $[\text{Ru}(\text{bpy})_3^{2+}]$ .<sup>22</sup> Most recently, we reported that this series of complexes showed significant changes in lifetime and emission wavelength when conjugated to lipids, in organic solvents, and when incorporated into lipid vesicles.<sup>23</sup>

The complexes were chosen to provide both different luminophores and anchoring motifs. The luminophores chosen were the diimine ligands, bipyridyl, and phenanthroline, and the binding motifs include single-point anchoring and double-point anchoring via the luminophore and through the ancillary phosphine ligands. Immobilization of the complexes on the SPC was accomplished using standard bioconjugation techniques. These same techniques were recently used to bind this series of complexes to both lipids and cholesterol.<sup>23</sup>

The surfaces used in this study were SPC made from both 300–500  $\mu\text{m}$  and 10–20 nm particles. The polyamines used

were high molecular weight (25 000) poly(ethylenimine) (PEI), which has the designation WP-1, and poly(allylamine) (PAA) (15 000 MW), which has the designation BP-1 after grafting to the silanized silica surface (Scheme 1). These designations are derived from the commercially produced materials made according to published patents.<sup>11</sup> We also report the immobilization of the complexes on a 3-amino-propylsilica composite to gauge the role of the polyamines in determining the photophysical properties of the SPC–Ru complex systems. In our previous studies we found that the complex  $[\text{Ru}(\text{bpy})_2(5\text{-amino-1,10-phenanthroline})][\text{PF}_6]_2$  (**5**)<sup>24</sup> did not exhibit the anomalous changes in lifetime and emission wavelength observed for the phosphine-substituted complexes. We therefore include here the results for immobilization of this complex on the SPC as well.

## RESULTS

**Synthesis.** The unbound complexes were synthesized based upon previously published work, in which the same family of complexes were synthesized and characterized with a TFA

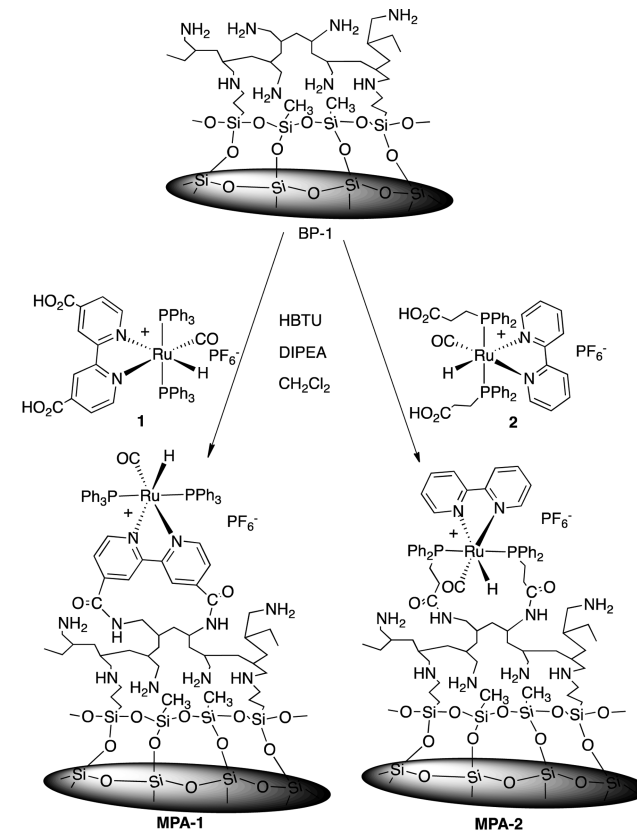
ligand instead of a hydride.<sup>22</sup> It was found that at higher temperatures (140 °C), over the 72 h reaction period, the complexes **1–4** and **4'** converted to a hydride via formation of an alkoxy complex, followed by  $\beta$ -hydride elimination.<sup>23</sup> This approach eliminated the extra step given in the paper<sup>22</sup> for converting the TFA to the hydride.

Using the published procedure<sup>23</sup> for synthesizing complex **4** was complicated by competitive formation of the corresponding acetal, **4'**, and by the fact that the compound and the acetal both exist as two isomers (see Chart 1 and Scheme S1 in the Supporting Information). The compounds **4** and **4'** could not be separated by chromatography on alumina. The presence of the acetal is confirmed by the presence of two singlets at  $\delta$  4.73 and 4.86 assignable to the CH proton in the two isomers that together integrate 1:2:2 with two multiplets at  $\delta$  3.45 and 3.70 (see Figure S1a). The aldehyde resonance appears as a broad singlet at  $\delta$  8.65, which is assigned to an overlap of the two aldehyde isomers (see Figure S1b). Integration of the aldehyde resonance relative to the two CH resonances of the acetal gives a ratio of approximately 2:3. The hydride resonances appear as a broad, equally spaced, asymmetric sextuplet centered at  $\delta$  –11.32, which we assign to an overlap of the expected four triplets of the two sets of two isomers (Figure S1b). The bipyridyl resonances also appear as overlapping doublets, and scaling the hydride to a value of one proton gives the correct integration for the overlapping bipyridyl and phenyl phosphine resonances, consistent with the presence of the two sets of two isomers (Figure S1b). The  $^{13}\text{C}$  NMR shows resonances entirely consistent with these assignments and the presence of the isomers (Figure S2). The quaternary phosphine carbon resonance in the  $^{13}\text{C}$  NMR appears as a triplet owing to the  $^{31}\text{P}$ – $^{31}\text{P}$  *trans*-virtual coupling and confirms the presence of two *trans* phosphines. The  $^{31}\text{P}$  NMR, however, shows only one overlapping resonance for the phosphines at  $\delta$  46 along with expected multiplet for the  $\text{PF}_6^-$  at  $\delta$  –139, which integrates 1:2 with the phosphine. A complete assignment of the NMR data along with relative integrated intensities for the various isomers is given in the Experimental Section. The formation of the acetal can be avoided by doing the reaction in toluene, but subsequent attempts to convert to the hydride in refluxing ethanol result in hemiacetal formation. On reaction with the SPC surface we see the formation of the imine based on the spectroscopic data by reaction of the aldehyde or the aldehyde and the acetal with the primary amine groups on BP-1 (*vide infra*).

The complex  $[\text{Ru}(\text{bpy})_2(5\text{-amino-1,10-phen})][\text{PF}_6]$  (**5**, Chart 1) and its photophysical properties have been previously reported.<sup>24</sup> We report here the immobilization of this complex on composite surfaces with the goal of determining the role of the ancillary ligands on the photophysical properties for the surface-bound complexes.

The three synthetic routes used to achieve binding of the ruthenium complexes onto the surface of the SPC particles are shown in Schemes 2–4. First, for the carboxylic acid linkers a peptide coupling reagent, HBTU, was used to facilitate a one-pot reaction that created an amide linkage between the surface and the complex.<sup>31,32</sup> Second, for the amine-to-amine coupling the complex was converted to an isothiocyanate derivative. This allowed reaction with the amine surface to form a covalent linkage via a stable thiourea bond.<sup>33</sup> Third, the carbaldehyde coupling occurred via direct reaction of the 4-methyl-2,2'-bipyridine-4'-carbaldehyde with the amine surface. This

**Scheme 2. Coupling of **1** and **2** to BP-1**



HBTU = O-(Benzotriazol-1-yl)-N,N,N',N'-tetramethyluronium hexafluorophosphate  
DIPEA = di-isopropylethyl amine

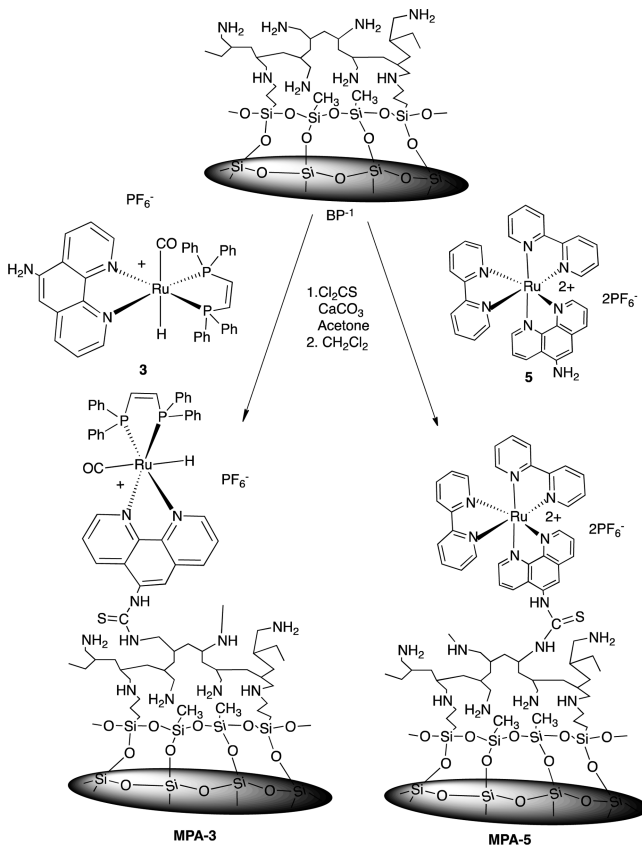
reaction was carried out in methylene chloride at room temperature.

**IR, NMR, and Solid-State NMR (SS-NMR).** The complexes in solution were previously characterized via IR and NMR, and these data are reviewed here for comparison with the surface-bound species.<sup>23</sup> All the complexes, except the trisdiimine complex **5**, showed a strong metal CO stretch between  $\sim$ 1940 and 2000  $\text{cm}^{-1}$ , as well as the strong diimine ring stretches between  $\sim$ 800 and 840  $\text{cm}^{-1}$ .  $^1\text{H}$  NMR showed the presence of a hydride, split as a triplet, at  $\delta$  –11.1 for the complexes **1** and **2** and  $\delta$  –6.9 ppm for complex **3**, while the  $^{13}\text{C}$  NMR showed CO peaks at  $\delta$  200–205, indicative of a metal-bound CO.  $^{31}\text{P}$  NMR showed a single doublet in the  $\delta$  40–50 range and the  $\text{PF}_6^-$  septuplet at  $\delta$  145, with a relative intensity ratio of 2:1.

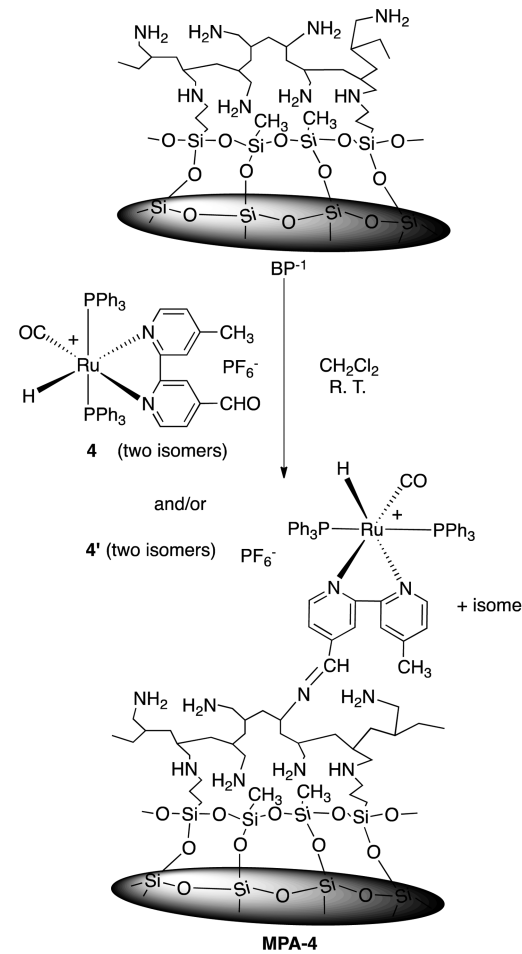
All the composites containing the immobilized complexes were characterized by IR and  $^{13}\text{C}$  and  $^{31}\text{P}$  SS-NMR, which confirmed the presence of the complex on the surface, except **MPA-5**, which was characterized only by IR and  $^{13}\text{C}$  SS-NMR. In the IR all the composites, except **MPA-5**, showed a weak CO stretching peak in the carbonyl, 1940–2000  $\text{cm}^{-1}$ , which corresponds to the same stretch as the complex in solution (Figure 1). In the case of **1** the band at 1729  $\text{cm}^{-1}$  is due to the carboxyl groups in **1**, and on reaction with the surface the carboxyl group is converted to an amide that shows a strong broad band at 1637  $\text{cm}^{-1}$  in **MPA-1**.

Each compound also shows a very strong band at  $\sim$ 840  $\text{cm}^{-1}$ , indicative of the diimine rings, which is consistent with the intact complex being on the surface. **MPA-2**, with its much longer tether, shows only one such band at 1640  $\text{cm}^{-1}$ . **MPA-1**,

Scheme 3. Coupling of 3 and 5 to BP-1



Scheme 4. Coupling of 4 and/or 4' to BP-1



NPA-1, and NPA-2 also show weak carboxylate ion stretches at 1530 and 1399  $\text{cm}^{-1}$ . Surprisingly, MPE-1 also shows only one amide CO stretch in this region at 1672  $\text{cm}^{-1}$ , where free carboxylate might be expected due to the lower number for primary amines (*vide infra*). Compounds MPA-3, NPA-3, and MPA-5 show the stretches for the C=S bond at 1399  $\text{cm}^{-1}$ , and a C=N bond can be seen and a 1630  $\text{cm}^{-1}$  imine bond in MPA-4.

$^{13}\text{C}$  SS-NMR resonances at  $\delta$  100–150 also confirmed the presence of aromatics on the surface. However, due to the broadness of the peaks, the difference between the diimine carbons and the phenyl groups on the phosphines are indistinguishable.  $^{13}\text{C}$  NMR of  $^{13}\text{CO}$ -enriched composites show the presence of the CO ligand at  $\delta$  200–210 in the composites tested (MPA-1–MPA-3).  $^{31}\text{P}$  SS-NMR of the complexes on the composites shows a single peak in a similar chemical shift range to that observed in solution. The presence of multiple spinning side bands suggests a high degree of anisotropy and that the complexes are in a fairly rigid environment (Figure 2). A complete set of  $^{13}\text{C}$  SS-NMR spectra for the complexes on the composites is provided in the Supporting Information.

$^{29}\text{Si}$  SS-NMR was performed primarily on the aminopropyl analogues for the micro- and nanoparticles and for the nanoparticle analogues of BP-1 and WP-1.  $^{29}\text{Si}$  SS-NMR of BP-1 and WP-1 microparticles have been previously reported.<sup>1,10</sup> The aminopropyl microparticles show a high ratio of T to Q peaks on the surface after reaction with aminopropyltrimethoxysilane. The T<sub>n</sub> peaks indicate a silica bound to one alkyl and *n* Si—O—Si bonds, while the Q peaks represent bulk silica (Q<sub>4</sub>) and surface silica having one (Q<sub>3</sub>)

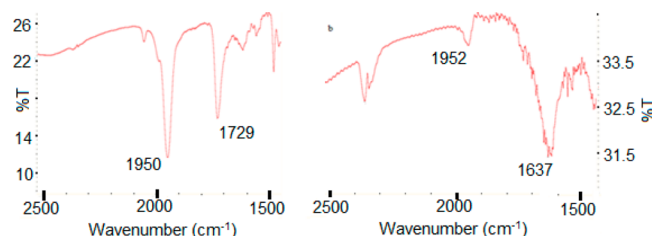


Figure 1. Comparison of metal–CO IR stretching frequency between (a) compound 1 as a KBr pellet and the analogue (MPA-1) on the BP-1 surface (b).

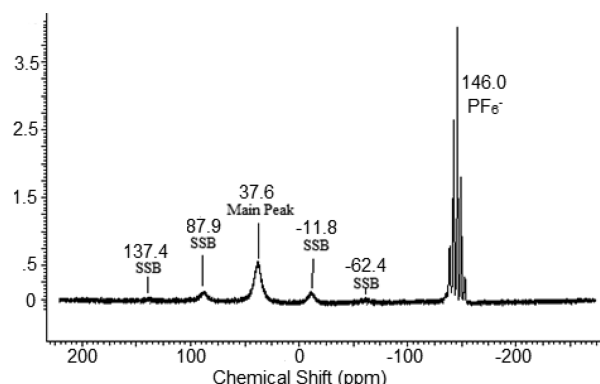
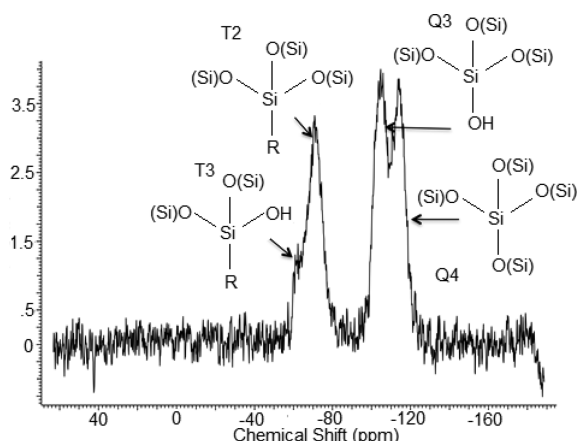


Figure 2. CPMAS  $^{31}\text{P}$  solid-state NMR of MPA-3 at 202.5 MHz.

and two ( $Q_2$ ) surface hydroxyl groups, respectively (Figure 3). The assignments for the different species vary only within 1–2



**Figure 3.** CPMAS- $^{29}\text{Si}$  SS-NMR showing the resonance peak differences between bulk and surface silanes.

ppm for different modified silicas, and those reported here are based on prior work.<sup>1,8</sup> In the case of the aminopropyl composites the ratio of T/Q decreases after reaction with the complexes, indicating that the surface aminopropyl groups are being lost due to hydrolysis during the reaction.

The hydrolysis of the groups is much greater for the nanoparticles, as shown by the complete disappearance of the T peaks in the  $^{29}\text{Si}$  SS-NMR and loss of the propyl chain carbons in the  $^{13}\text{C}$  SS-NMR (Figure 4). We suggest that this is due, in part, to the nanoparticles' spherical shape and small size, which results in a large curvature, allowing easier access of nucleophiles (the isothiocyanate in the case of complex 3) to

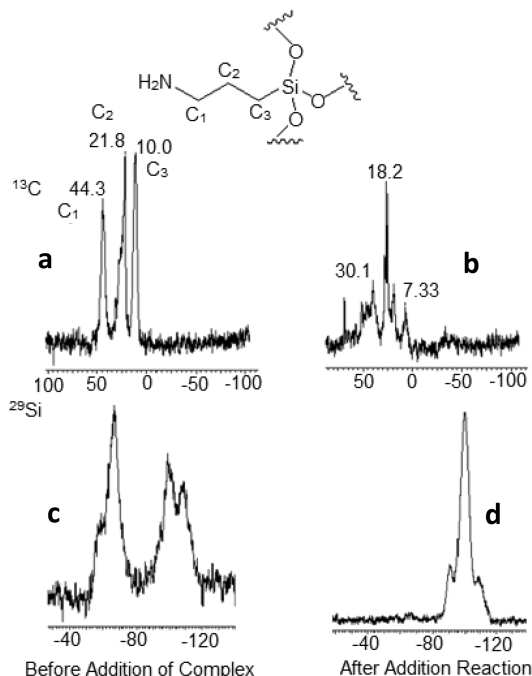


**Figure 4.** (a)  $^{13}\text{C}$  of NPA prior to reaction with complex 3. (b)  $^{13}\text{C}$  of NPA after reaction with complex 3 showing loss of the aminopropyl groups. (c)  $^{29}\text{Si}$  SS-NMR of NPA prior to reaction with complex 3. (d)  $^{29}\text{Si}$  SS-NMR after reaction with complex 3 showing loss of  $T_n$  sites.

the surface Si–O bonds, thereby enhancing hydrolysis. The relatively flat sections of the much larger microparticles allow the aminopropyl groups to pack more tightly and provide a more protective layer.

**Loading.** The loading of the complexes on the SPC was evaluated by atomic absorption analysis of the Ru content after complete digestion of the samples. The microparticles MPA-1, MPA-2, and MPA-3 load at 0.039, 0.013, and 0.044 mmol/g, respectively, while the nanoparticle analogues NPA-1, NPA-2, and NPA-3 load at 0.048, 0.015, and 0.023 mmol/g, respectively. The loadings are similar except in the case of the aminophenanthroline analogues, where loading is significantly higher for the microparticles (Figure 5). These loadings

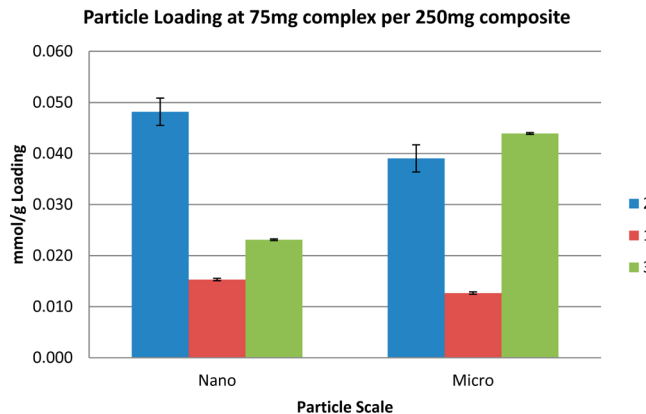


**Figure 5.** Bar graph showing the loading levels of complexes 1–3 on micro and nano SPCs.

are in the range 1–3% based on the mmol of N per gram of BP-1 (1.6 mmol/g) and do not compare favorably with the ligand loadings of ligands such as chloroacetate, where loadings are in the range 40–70% of the available amines on similar composites.<sup>34</sup> This is not too surprising in light of the greater bulk of the complexes 1–3 and the lower efficiency of the linker chemistry compared with simple nucleophilic displacement chemistry used with chloroacetate.

The loading studies also revealed that the complexes coupled to the surface with HBTU reach a saturation point after which no further loading is realized. For the nanoparticles, once the ratio of complex to composite reaches 75 mg per 250 g of composite, loading actually decreases. This is likely due to the higher base concentration required for the coupling reaction. This causes increased degradation of the surface in the case of the more sensitive nanocomposites (Figure 6).

**Luminescence Studies.** The emission of the complexes was measured by irradiation at 470 nm using the configuration described in the Experimental Section. This wavelength targets the metal-to-ligand charge-transfer band (MLCT) usually found between 430 and 470 nm.<sup>23,27</sup> The MLCT bands for the complexes reported here in solution are given in Table 1.

Attempts to measure the absorption spectra of the particles using diffuse reflectance techniques were unsuccessful. However, MPA-1 was sent to Online Instrument Systems (OLIS), and using their CLARiTY absorbance spectrometer they measured the absorbance spectra of 1 on the BP-1 surface. A comparison of the MLCT bands observed in solution and on the composite surface is shown in Figure 7. Both show absorption maxima in the same MLCT region. The surface-bound MPA-1, however, shows two partially resolved bands,

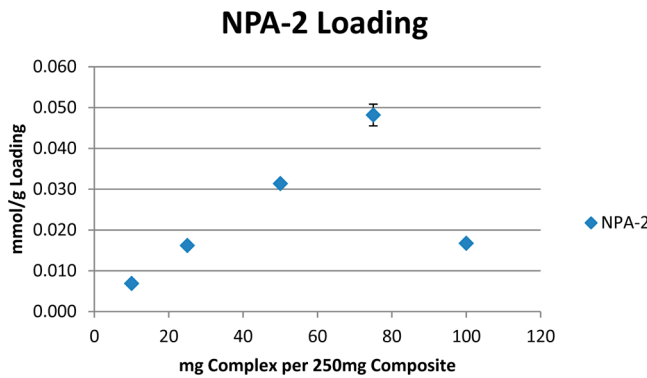


**Figure 6.** Graph showing the loading levels of complex 2 on reaction with NPA.

**Table 1. Comparison of Emission Maxima for Complexes in Solution and Complexes on BP-1**

compound	emission maximum (nm) in ETOH solution	emission maximum (nm) on BP-1
MPA-1	647	634
MPA-2	600	600
MPA-3	590	590
MPA-4	612	604
MPA-5	635	612

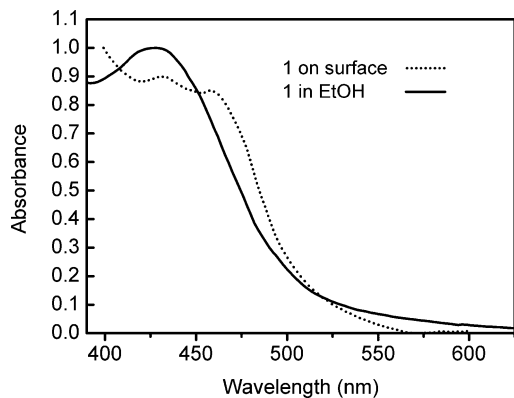


**Figure 7.** Absorption spectra of complex 1: in solution (---); on the composite BP-1 (MPA-1) (—).

while **1** in solution shows one maximum. This could be due to vibronic structure, electronic bands becoming apparent due to environment-dependent shifts and band narrowing, or the presence of several differently bound species; it has been observed in solution for some of these complexes (Figure 7).<sup>22,23,27–29</sup>

Complexes **1**, **4**, and **5** showed small but significant changes in their emission wavelength on binding to the BP-1 surface, while **2** and **3** showed emission wavelengths identical to those observed in the solution (Table 1). The shape of the emission curves is the same in both cases, and this is illustrated for **2** and MPA-2 in Figure 8 (top).

From the excitation spectra, it is observed that the major contribution to the excited state comes from the MLCT absorption band, as expected, but in the case of complexes **1**–**4** there is an additional contribution from absorption bands at 280 and 350 nm that can be assigned to the intraligand transitions on the diimine and phosphine ligands both in solution and on the surface (Figure 8b). Interestingly, for the

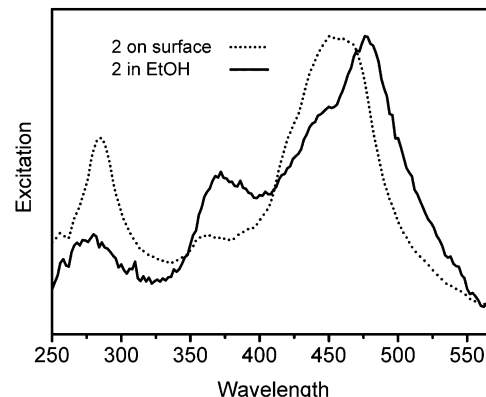
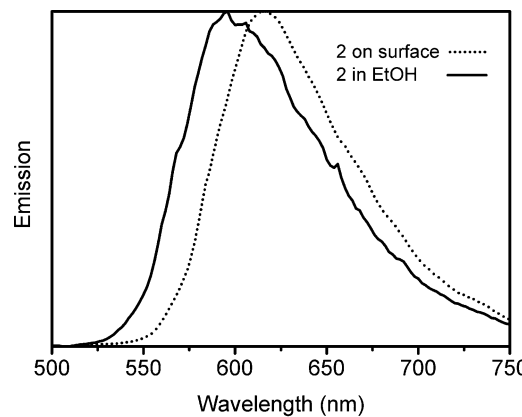


**Figure 8.** Top: Peak normalized emission spectra of complex 2 in solution (—) and on the composite BP-1 (MPA-2) (----). Bottom: Excitation spectra of complex 2 in solution (—) and on the composite BP-1 (MPA-2) (----).

surface-bound complex **2** the contribution from the diimine ligand noticeably increases, while that of the band at 350 nm decreases (Figure 8, bottom). These changes report on the relative efficiencies of pathways populating the emissive state from the optically populated ones. From Figure 8 bottom, it follows that population of the emitting  $^3\text{MLCT}$  from the intraligand state excited around 280 nm is more efficient than in solution. In the case of **5**, which does not have phosphine ligands, the excitation spectra show only contributions from transitions around 300 nm.<sup>23</sup> The broadening of the excitation spectrum on the surface relative to solution is indicative of a very heterogeneous environment (Figure 8, bottom).

The emission wavelengths for the complexes **1**–**4** coupled to the silica nanoparticles (NPA-1–NPA-4) were identical to those on the microparticles (MPA-1–MPA-4), and their excitation spectra are similar. In the case of the complexes **1**, **3**, and **4** coupled to the branched polymer composite WP-1 (MPE-1, MPE-3, and MPE-4) the emission wavelength of MPE-1 shifts to 616 nm from 634 nm in MPA-1, while the other two complexes had the same emission maximum as MPA-3 and MPA-4. Complexes **2** and **3** were also coupled to aminopropyl-modified silica microparticles. Complex **2** on this surface (MAP-2) showed a shift to 616 nm from 600 nm, also observed for MPA-2, while complex MAP-3 had the same emission as MPA-3. These data indicate that, in general, the surface environment has only a slight effect on the emission wavelength relative to the complex in solution, which suggests that the transition energies of the metal and the ligands are relatively insensitive to surface immobilization.

**Lifetime Measurements.** A comparison of the excited-state lifetimes of the complexes **1–5** in solution and on the composite BP-1 is shown in Table 2. The multiple exponentials

**Table 2. Comparison of Lifetimes for Complexes in Solution and Complexes on BP-1 Microparticles**

compound	lifetime (ns) <sup>a</sup> in ETOH solution	lifetime on BP-1 (PAA) <sup>a,b</sup> (μs)	lower and upper 95% confidence limits on BP-1 (μs)
MPA-1	720	3.45 (4.8× increase)	3.29/3.63
MPA-2	236	1.28 (5.4× increase)	1.26/1.30
MPA-3	240	0.93 (3.9× increase)	0.85/1.01
MPA-4	225	1.43 (6.3× increase)	1.30/1.57
MPA-5	220	0.270 (1.2× increase)	0.250/0.330

<sup>a</sup>Lifetimes are reported as intensity-average values. <sup>b</sup>Increases are calculated as ratio of composite lifetime/solution lifetime.

associated with the lifetime measurements of the systems studied here reflect the complex heterogeneity of the local environments. This heterogeneity can arise from a number of sources including different local interactions with the matrix. As such it is expected that the decay will be complex, and it would be difficult, if not impossible, to attribute physical meaning to each component resolved from fitting to a sum of exponentials. Therefore, for the purpose of this study, the relevant observable is the persistence time in the excited state of a probe on a particular matrix, which is defined by the intensity-average lifetime (eq 2 in the Experimental Section).

It can be seen that, with the exception of **5**, all the complexes show increases in the intensity-average lifetime 4- to 6-fold that in solution (Table 2).

The observed large increases in lifetime likely arise from several factors. First, limiting the accessible vibrational modes will reduce internal conversion and lengthen lifetime. Second, lifetime lengthening upon surface binding can also be due to lack of solvation, because coupling of molecular and solvent vibrational modes provides an effective deactivation pathway. This is a well-known effect, observable also when transition-metal chromophores are placed in constrained supramolecular media. The magnitude of the increase is large and potentially useful in electron transfer chemistry.

In comparison with the other complexes, **5** showed only a slight increase in lifetime. This could be due to a number of factors. First, the molecular volume of **5** is much less than the other complexes, which would lead to less steric interaction with the surface and relatively greater mobility (Figure 9).

Increased solvent collisions or easier population of deactivating dd states would result in quenching and faster decay. Second, the likely electron acceptor ligands in **5** are the bipyridyl ligands, and the absence of the phosphines could result in less electron delocalization in the excited state, making the complex less sensitive to changes in accessible modes of relaxation. These interpretations, however, must be considered only tentative, as the factors contributing to excited-state lifetimes are many and complex.<sup>23,27</sup>

To gain a better understanding of how the nature of the surface influences the excited-state lifetime of the immobilized complexes, we have compared the lifetime of the single-tethered complex **3** on BP-1, WP-1, and aminopropyl microparticles. BP-1 is made with the linear PAA and has pendent primary amine groups. WP-1 is a branched polymer consisting of approximately equal amounts of primary, secondary, and tertiary amine groups with the secondary and tertiary amines in the backbone of the polymer, a much more rigid network, overall; the aminopropyl group probably provides the most flexible environment for the immobilized complex. On the PEI-coated microparticles the single-anchor complex **3** showed an increase in average lifetime, on the order of 8× compared with that of the complex in solution. The aminopropyl- and PAA-modified surfaces showed smaller increases in average lifetime, indicating that local mobility is a determining factor for the observed increases in lifetime (Scheme 5). Complex **3** bound to the most flexible surface, aminopropyl, showed a significantly larger increase relative to the same complex on the linear polymer PAA. This could be the result of direct interactions of the complex with the silica surface, a phenomenon noted with other aminopropyl-modified silicas.<sup>35</sup>

We then examined the lifetime of two other complexes, **1** and **4**, on the more rigid surface of WP-1. These complexes showed respectively only about half to 3-fold increases in average lifetime, less than that observed on BP-1 (Table 3).

This is likely due to the fact that the isothiocyanate can react with secondary as well as primary amines, while the carboxylate and carbaldehyde linkers in **1** and **4** react only with primary amines. As a result, complex **3** is at least partially bound to secondary amines (~30–35% of the total) in the PEI polymer backbone, therefore giving an intensity-averaged lifetime that is much longer than that of the other two complexes, which can react only with the more mobile terminal primary amines. Although **1** has two potential tethers that would be expected to result in less surface mobility, in WP-1 the primary amines (~30–35% of the total) are present on the surface at widely

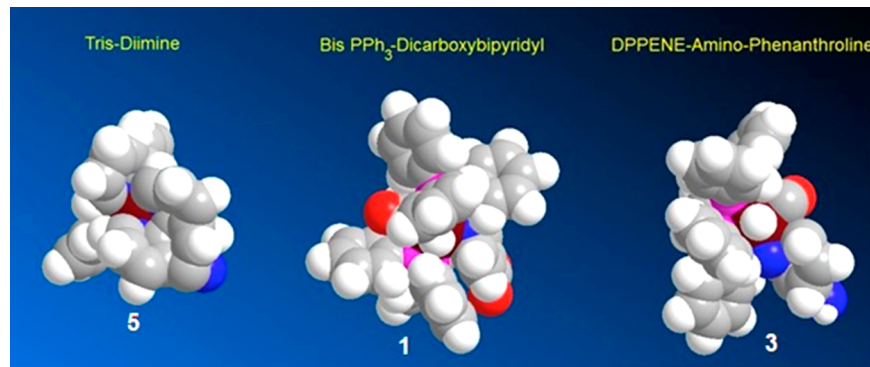


**Figure 9.** Close-packed sphere models of complexes **5**, **1**, and **3**.

Scheme 5. Lifetimes of Complex 3 on Different Surfaces

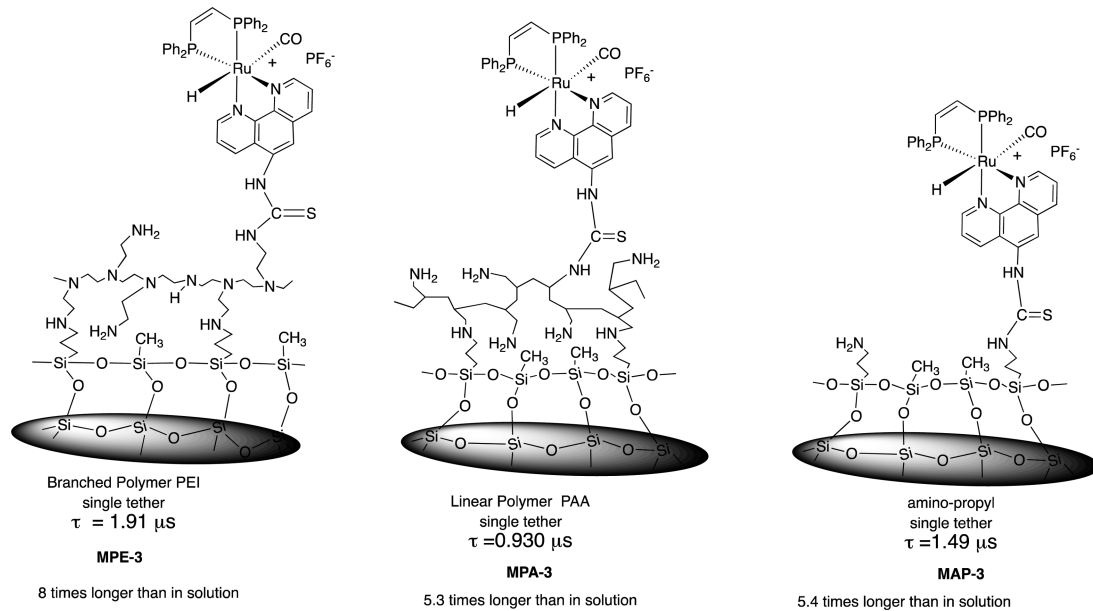


Table 3. Comparison of Lifetimes for Complexes on Different Microparticle Surfaces

compound	lifetime on WP-1 (PEI) MPE-1, MPE-3, MPE-4 ( $\mu\text{s}$ ) <sup>a,b</sup>	lower and upper 95% confidence limits ( $\mu\text{s}$ )	lifetime on amino-propyl MAP-2, MAP3 ( $\mu\text{s}$ ) <sup>a,b</sup>	lower and upper 95% confidence limits ( $\mu\text{s}$ )
1	1.02 (1.4× increase)	0.90/1.15		
2			1.20 (5.1× increase)	0.99/1.4
3	1.91 (8× increase)	1.86/2.01	1.49 (6.2× increase)	1.17/1.92
4	0.71 (3.1× increase)	0.66/0.75		

<sup>a</sup>Lifetimes are reported as intensity-average values. <sup>b</sup>Increases are calculated as ratio of composite lifetime/solution lifetime.

spaced intervals, and statistically it is likely that only one of the two tethers is surface bound at each site. That the lifetime of 1 on the more rigid WP-1 is shorter than on BP-1 could be due to the fact that the primary amines in PEI are linked to the backbone by a two-carbon tether, while in BP-1 the amine is linked to the backbone by a one-carbon tether. These studies indicate that it is the structure of the polymer and its relative rigidity on the surface rather than the type of tether on the complex that is more important in determining the extent of the increases in the average excited-state lifetime.

To gain insight as to how particle size and shape influence the excited-state lifetimes of the immobilized complexes, photophysical measurements were performed on complexes 1–4 immobilized on silica nanoparticles modified with PAA (*vide supra*). The emission spectra for these complexes on the nanoparticles were identical with those on the microparticles. The lifetimes measured for NPA-1, NPA-2, NPA-3, and NPA-4 were 1.59, 1.51, 0.880, and 0.550  $\mu\text{s}$ , respectively, which gave the ratios of 2.2, 6.3, 3.6 and 2.5× compared with the lifetimes of the complexes in solution (Table 4).

This suggests that surface shape has a significant influence on the excited-state lifetime. The microparticles have a local surface that at any given point is relatively flat compared with the radii of the complexes. However, due to the small size of the nanoparticles there is a significant local curvature that can affect interaction of the complexes with the surface. In the case of complex 2, the longer tether is able to extend around the curvature in order to get both anchors attached. By contrast, the shorter tethered dicarboxylate linker in 1 can anchor at only one point due to the small radius of curvature of the

Table 4. Comparison of Lifetimes for Complexes in Solution and Complexes on BP-1 Nanoparticles

compound	lifetime ( $\mu\text{s}$ ) <sup>a,b</sup>	lower and upper confidence limit ( $\mu\text{s}$ )
NPA-1	1.59 (2.2× increase)	1.37/1.90
NPA-2	1.51 (6.3× increase)	1.30/1.74
NPA-3	0.88 (3.6× increase)	0.65/1.20
NPA-4	0.55 (2.5× increase)	0.50/0.55

<sup>a</sup>Lifetimes are reported as intensity-average values. <sup>b</sup>Increases are calculated as ratio of composite lifetime/solution lifetime.

nano-particles. This is consistent with the higher loading of 2 on the nano- and microparticles relative to 1. In the case of complex 3 on the nanoparticles, the loading is about half that of the microparticles (Figure 6). Although both loadings are quite low relative to the available amines, the lower loadings apparently result in a higher mobility on the surface and smaller increases in lifetime. Furthermore, the greater curvature of the nanoparticles could result in less surface interaction of the bulky phosphines with the poly(allylamine), and that would increase surface mobility.

## CONCLUSIONS

The results of this study have shown that binding of an organometallic ruthenium complex to a surface does not significantly affect its absorbance or emission properties. This indicates that interactions with the polyamine and amino-propyl/silica surfaces do not affect the transition energies involved in the MLCT bands of these complexes. However, the average excited-state lifetime is markedly affected. The studies

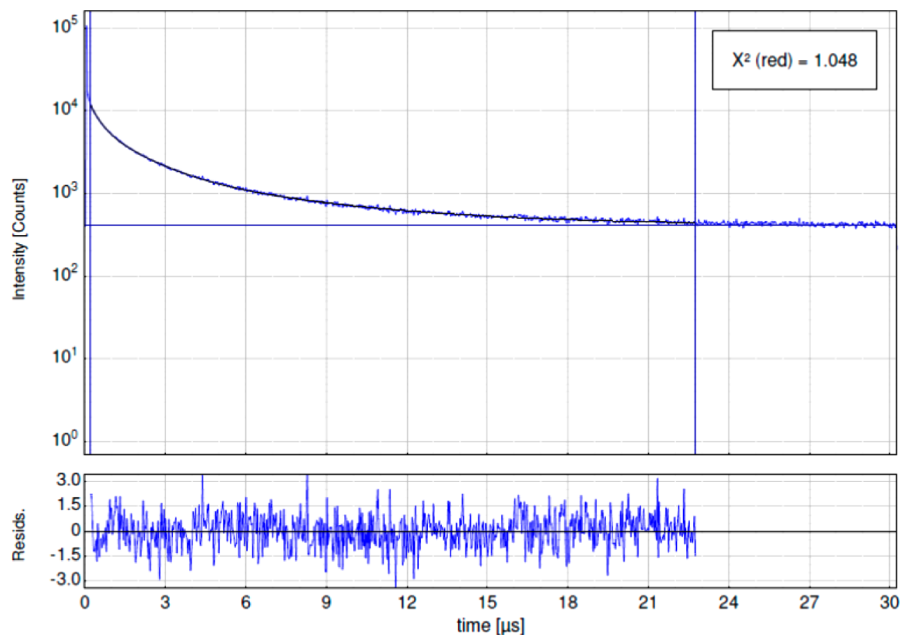


**Figure 10.** Lifetime decay curve for MPA-1, with a fitted average lifetime of  $3.45\ \mu\text{s}$ .

reported here suggest that the relative rigidity of the surface is a major contributor to this phenomenon. In addition, there are significant differences between the excited-state lifetimes when on micro- versus nanoparticles. We have tentatively assigned these differences to the different surface shapes of the micro- and nano-SPC.

In the case of complex **5**, there is only a slight difference in excited-state lifetime relative to its solution value. This result points to the importance of the ancillary ligands in increasing the excited-state lifetime of the immobilized complex. The origin of this effect could be steric or electronic, or both. Complex **5** has a smaller molecular volume than the phosphine-containing complexes, as can be seen from the closed-packed, hard-sphere models shown in Figure 9. Thus, the bulky phosphines could interact more with the surface polyamine, for example, while **5** might move more freely on the surface. On the other hand, excited-state lifetimes are subject to a number of electronic effects. The excitation spectra clearly indicate the participation of the phosphine ligand in the MLCT, and this affects the degree of spin-orbit coupling, delocalization of electron density in the excited state, and the perturbation of LUMO and HOMO energies. We have observed differences in the photophysical properties between **5** and complexes **1–3** on bioconjugation and on incorporation into liposomes, which perhaps are related electronic effects.<sup>23</sup> These are complex issues that might be addressed by TDDFT in combination with molecular mechanics calculations. This is planned for the future.

These studies open the door for detailed investigation of the electron transfer properties of the immobilized complexes **1–4**. The longer lifetimes promise lower activation energies for electron transfer, which could increase the rates of carbon dioxide reduction, a transformation where ruthenium diimine complexes have been shown to be promising.<sup>36</sup> The complexes are air stable and, so far, show no decomposition when irradiated after immobilization on SPC.<sup>12,21,22</sup> These studies are under way in our laboratory.

## EXPERIMENTAL SECTION

**Materials.** Tetrahydrofuran was distilled from sodium/benzophenone, and methylene chloride and acetonitrile were distilled from calcium hydride. Ruthenium carbonyl was purchased from Strem Chemicals. Diisopropyl ethyl amine (DIPEA), 4,4'-dicarboxy-2,2-bipyridyl(DcBpy), 3-Diphenylphosphino propionic acid (DPPA), 5-amino-1,10-phenanthroline, 4,4'-dimethyl-2,2'-bipyridyl, and O-benzotriazole-N,N,N',N'-tetramethyluroniumhexafluorophosphate (Aldrich) were used as received. The SPC, BP-1, and WP-1 microparticles were synthesized by previously reported methods using a 7.5:1 mixture of methyltrichlorosilane and 3-chloropropyltrichlorosilane for the silanization step.<sup>10</sup> Silica gel (26.7 nm average pore diameter, 2.82 mL/g pore volume, 84.7% porosity, 422 m<sup>2</sup>/g surface area) was obtained from INEOS Enterprises Ltd, UK, and was sieved to 300–550 μm. The SiO<sub>2</sub> nanoparticles (10–20 nm) (Aldrich) were dried at ~200 °C before use. The polymers poly(allylamine) (PolySciences, MW = 15 000) and poly(ethylenimine) (Aldrich, MW = 25 000) and the monomer aminopropyltrimethoxysilane (Alfa Aesar) were used as received. The aminopropyl-modified micro and nano silica composites were synthesized according to published literature procedures.<sup>25</sup> Complexes **1–3**, **3'**, and **5** were synthesized by published literature procedures.<sup>23,24</sup> Silanization of the nanoparticles was done according to published literature procedures with the addition of sonication of the reaction mixtures.<sup>10</sup>

**Spectroscopic Measurements.** <sup>1</sup>H and <sup>31</sup>P solution NMR were performed on a Varian NMR Systems spectrometer at 500 and 202.6 MHz, respectively. Solid-state CPMAS <sup>13</sup>C, <sup>31</sup>P, and <sup>29</sup>Si NMR were obtained on the same spectrometer at 125, 202.5, and 99.4 MHz, respectively, using a 4 mm rotor at a spin speed of 10 kHz. IR spectra were taken on a Thermo-Nicolet 633 FT-IR spectrometer as KBr pellets. Luminescence data were obtained on a Molecular Devices Spectra Max M2, and by using double-sided carbon tape silica particles were mounted on a glass slide cut to the size of the 1 cm cuvette holder. The angle of the glass slide relative to the excitation beam was adjusted to give maximum emission. Absorbance spectra for the coated silica particles were performed at OLI Systems using a CLARiT<sup>Y</sup> spectrometer and were run as suspensions in glycerol.

**Metal Analysis.** Ruthenium loading data were determined by atomic absorption on an S series Thermo Electron Corporation AA spectrometer after digesting the silica particles. The digestion was performed by first calcining 40 mg of the coated particles in an oven at 500 °C overnight. The calcined particles were then transferred to

polypropylene tubes, combined with 0.5 mL of concentrated HF acid and 0.5 mL of modified aqua regia (6:1 concentrated HCl acid/HNO<sub>3</sub> acid), and diluted to 4.5 mL total volume with DI water.<sup>26</sup> After dilution each sample was vortexed until particles had completely dissolved and the solution was translucent. Each sample was run in duplicate, and standards were run approximately every 12 samples, spanning a linear range on the AA spectrometer of 5–50 ppm.

**Excited-State Lifetime Measurements.** Time-resolved luminescence decay measurements were performed by time-correlated single-photon counting (TCSPC), using the Quantum Northwest FLASC 1000 fluorimeter (Spokane, WA, USA). The dry silica particles were held in place by double-sided carbon tape on the surface of a triangular cuvette 45° to the incident beam. Pulsed excitation at 470 nm and a repetition rate of 50 kHz (external trigger) from a LDH-P-C 470 laser diode (PicoQuant, Berlin, Germany) were used to excite the complexes for time-dependent studies. In the FLASC 1000 the luminescence decays were collected orthogonal to the excitation beam path and at the magic angle polarization condition<sup>27,28</sup> using a 620/50 nm bandpass filter (Chroma, Rockingham, VT, USA) to isolate the emissions and eliminate excitation scatter. Measurements were taken at room temperature under ambient air conditions. The decay curves were collected until  $4 \times 10^4$  counts were reached using the NanoHarp 250 PCI board (PicoQuant, Berlin) with a timing resolution of 560 ps/channel. Luminescence lifetimes were determined using the FluoFit Pro V4.2.1 (PicoQuant, Berlin) analysis software package<sup>29a</sup> and reported as the intensity average based on a multiexponential model, where the magic-angle intensity decay is given by

$$I(t) = \sum_{i=1}^n \alpha_i e^{-t/\tau_i} \quad (1)$$

In this model,  $\tau_i$  is the lifetime and  $\alpha_i$  is the amplitude of the  $i$ th component, and the intensity-average lifetime is given by

$$\langle \tau \rangle = \frac{\sum \alpha_i \tau_i^2}{\sum \alpha_i \tau_i} \quad (2)$$

The estimated error in the average was calculated from the upper and lower 95% confidence limits of the individual decay components, which were determined by the support-plane method.<sup>29b</sup>

A representative decay curve and the goodness to fit are shown above as Figure 10.

**Synthesis.** All reactions were carried out under an inert atmosphere, N<sub>2</sub> or Ar, except during washes and any purification procedures. Overhead stirring was used for all the reactions involving the SPC microparticles, as this minimizes particle fragmentation. Sonication of the nanoparticle reactions was carried out with a VWR B1500A-MTH sonicator.

**Composite Nomenclature.** The composites are named by the first two letters of the polymer or aminopropyl to which the complex is bound: PA for PAA (BP-1); PE for PEI (WP-1); and AP for aminopropyl. The microparticle composites have the letter prefix M (e.g., MPA), and the nanoparticles have the letter prefix N (e.g., NPA). The complex is designated by its number (e.g., MPA-1 means complex 1 bound to PAA on the microparticle BP-1, SPC).

**Synthesis of trans-[(H)Ru(CO)(4'-methyl-2,2'-bipyridine-4-carbaldehyde)(PPh<sub>3</sub>)][PF<sub>6</sub>] (4) and trans-[(H)Ru(CO)(4'-methyl-2,2'-bipyridine-4-ethylene glycol acetal)(PPh<sub>3</sub>)][PF<sub>6</sub>] (4').** The ligand 4'-methyl-2,2'-bipyridine-4-carbaldehyde (mbpyc) was synthesized according to previously published procedures.<sup>30</sup> A 250 mg sample of Ru(CO)<sub>2</sub>(PPh<sub>3</sub>)<sub>2</sub>(TFA)<sub>2</sub><sup>22</sup> (0.28 mmol) and 70 mg (0.28 mmol) of mbpyc were combined in 20 mL of ethylene glycol. The mixture was heated to 140 °C and stirred for 72 h. After 72 h the reaction was cooled to room temperature and the compound was precipitated from solution by the dropwise addition of 1 mL of an aqueous solution of NH<sub>4</sub>PF<sub>6</sub> containing 1 g/10 mL. The precipitate was collected by centrifugation at 3000 rpm, washed 2× in DI H<sub>2</sub>O, followed by centrifugation, and then washed 1× with diethyl ether. Following the ether wash and rotary evaporation the product was dissolved in 5:2:2 hexane/MeOH/CH<sub>2</sub>Cl<sub>2</sub> and then chromatographed on neutral alumina using the same solvent as eluent. A single product

band containing 4 and 4' was obtained (35 mg, 13%). IR in KBr: 1986 (vs), 1614 (vs) 1435 (m) 836 (vs). <sup>1</sup>H, <sup>13</sup>C, <sup>31</sup>P, and <sup>19</sup>F NMR spectra are shown in the Supporting Information (Figures S1–S4). NMR data in CD<sub>2</sub>Cl<sub>2</sub>. <sup>1</sup>H NMR shifts ( $\delta$ , relative to TMS): aldehyde proton: 8.65 (bs, 0.4H); bipyridyl protons: 8.65 (d, 1H), 8.49 + 8.41 (2d, 1H), 6.98 + 6.91 (2d, 1H), 6.27 + 6.19 (2d, 1H); phosphine phenyl protons: 7.6–7.2 (m, 32H, includes 2 overlapping bipyridyl protons); acetal protons: 4.86 (s, 0.3H) 4.73 (s, 0.3H) 3.70 (m, 0.6H) 3.45 (m, 0.6H); acetal methyl protons: 2.54 (s, 0.9H), 2.50 (s, 0.9H) aldehyde methyl protons: 2.48 (s, 0.6H), 2.43 (s, 0.6H), hydride: -11.32 (m, 1H). <sup>13</sup>C NMR shifts ( $\delta$  relative to TMS): metal CO: 205.2; 8 bipyridyl quaternary carbons: 155.07, 154.77, 154.26, 154.08, 151.91, 151.49, 151.26, 150.92; 8 bipyridyl CH carbons: 127.82, 127.56, 125.84, 125.69, 124.26, 123.99, 122.00, 121.79; aldehyde: 152.6, 152.5; PPh<sub>3</sub> quaternary carbons: 132.20(t); PPh<sub>3</sub> CH + 4 bpy CH carbons: 133.65, 130.61, 128.92; acetal CH: 73.98 (bs); acetal carbons: 70.61 (CH), 70.35 (CH), 61.46 (CH<sub>2</sub>), 61.35 (CH<sub>2</sub>); methyl: 21.3, 21.2. <sup>31</sup>P NMR shifts ( $\delta$  relative to external H<sub>3</sub>PO<sub>4</sub>): PPh<sub>3</sub>, 46.04 (2P), PF<sub>6</sub><sup>-</sup>, 139 (1P). <sup>19</sup>F NMR shifts ( $\delta$  relative to external CFCl<sub>3</sub>): PF<sub>6</sub><sup>-</sup> : -74(d).

**General Procedure for Coupling of Complexes 1 and 2 to the Composites with HBTU:**<sup>31,32</sup> **Synthesis of MPA-1, MPE-1, MPA-2, MAP-2, NPA-1, and NPA-2.** A 75 mg amount of complex 1<sup>22</sup> (0.07 mmol) was dissolved in 20 mL of CH<sub>2</sub>Cl<sub>2</sub> in a round-bottom flask, along with 35 mg of HBTU (0.09 mmol) and 0.09 mL of DIPEA (0.5 mmol). The reaction mixture was top stirred for a 30 min activation period at 25 °C, after which 250 mg of BP-1 microparticles was added to the flask. Following the addition of the BP-1, the reaction mixture was top stirred for an additional 3 h. The reaction was then stopped by removing the solvent from the particles, ~20 mL of MeCN was added, and the mixture was stirred for 1 h. This process was repeated three times, after which the particles were collected and dried on a vacuum line.

**Spectroscopic Data for MPA-1.** IR in KBr: 2956 (m, C-H), 2926 (m, C-H), 1952 (w, metal CO), 1637 (s, amide CO), 1620 (m, amide CO), 1534 (w, carboxylate ion), 1399 (w, carboxylate ion), 840 (s, diimine ring) cm<sup>-1</sup>. <sup>31</sup>P{<sup>1</sup>H} SS-NMR:  $\delta$  44.2, -145. <sup>13</sup>C{<sup>1</sup>H} SS-NMR:  $\delta$  203 (metal CO), 170–160 (amide), 150–110 (aromatics), 55–20 (polymer), -6 (Si-Me).

**Spectroscopic Data for MPE-1.** IR in KBr: 2964 (m, C-H), 2918 (m, C-H), 1938 (w, metal CO), 1672 (s, amide CO), 800 (s, diimine ring). <sup>31</sup>P{<sup>1</sup>H} SS-NMR:  $\delta$ : 46, -145. <sup>13</sup>C{<sup>1</sup>H} SS-NMR:  $\delta$  203 (metal CO), 160–170 (amide), 150–120 (aromatics), 50–20 (polymer), -6 (Si-Me).

**Spectroscopic Data for MPA-2.** IR in KBr: 2926 (m, C-H), 1944 (w, metal CO), 1674 (s, amide CO), 799 (s, diimine ring) cm<sup>-1</sup>. <sup>31</sup>P{<sup>1</sup>H} SS-NMR:  $\delta$  38, -145. <sup>13</sup>C{<sup>1</sup>H} SS-NMR:  $\delta$  203 (metal CO), 170–160 (amide), 150–110 (aromatics), 60–15 (polymer), -6 (Si-Me).

**Spectroscopic Data for NPA-1.** IR in KBr: 2926 (m, C-H), 1947 (w, metal CO), 1672 (s, amide CO), 1558 (w, carboxylate ion), 1397 (w, carboxylate ion), 840 (s, diimine ring) cm<sup>-1</sup>. <sup>31</sup>P{<sup>1</sup>H} SS-NMR:  $\delta$  38, -145. <sup>13</sup>C{<sup>1</sup>H} SS-NMR:  $\delta$  170–160 (amide), 150–110 (aromatics), 11.1 (C<sub>1</sub>), 21.5 (C<sub>2</sub>), 44.6 (C<sub>3</sub>) (aminopropyl chain).

**Spectroscopic Data for NPA-2.** IR in KBr: 2924 (m, C-H), 1956 (w, metal CO), 1733 (w) 1646 (s, amide CO), 1540 (w, carboxylate ion) 1399 (w, carboxylate ion), 798 (s, diimine ring) cm<sup>-1</sup>. <sup>31</sup>P{<sup>1</sup>H} SS-NMR:  $\delta$  46, -145. <sup>13</sup>C{<sup>1</sup>H} SS-NMR:  $\delta$  203 (metal CO), 170–160 (amide), 155–110 (aromatics), 44.8 (C<sub>3</sub>), 24.3 (C<sub>2</sub>), 8.6 (C<sub>1</sub>) (aminopropyl chain), 50–15 (polymer), -6 (Si-Me).

**General Procedure for Coupling Complexes 3 and 5 to the Composites via the Isothiocyanate Intermediate:**<sup>23,33</sup> **Synthesis of MPA-3, MPE-3, MPA-5, and NPA-3.** A 75 mg (0.13 mmol) portion of complex 3<sup>23</sup> was dissolved in 3 mL of dry acetone. Finely crushed CaCO<sub>3</sub> (30 mg, 0.45 mmol) was added to the solution followed by addition of thiophosgene (7.5  $\mu$ L, 0.07 mmol). The reaction mixture was stirred at room temperature for 1 h and then refluxed for 2.5 h. After cooling to room temperature, CaCO<sub>3</sub> was removed using a 0.45  $\mu$ m filter, and acetone removed by rotary evaporation. Compound [(H)Ru(CO)(dppene)(1,10-phen-5-NCS)]-

$[\text{PF}_6]$  ( $3'$ )<sup>23</sup> was obtained in 94% yield. IR in KBr: CO stretching frequency at 1990 (vs), N=C=S at 2119 (m) and 2046 (m)  $\text{cm}^{-1}$ .

Conversion of  $3'$  to  $3$  was performed by dissolving 75 mg of  $3'$  in 20 mL of  $\text{CH}_2\text{Cl}_2$  in a round-bottom flask, along with 250 mg of BP-1 microparticles. The reaction mixture was stirred at 25 °C overnight. The reaction was stopped by separating the particles from the solvent and washing 3× with fresh 20 mL aliquots of  $\text{CH}_2\text{Cl}_2$  with stirring for 1 h each wash. After washing, the particles were collected and vacuum-dried.

**Spectroscopic Data for MPA-3.** IR in KBr: 2924 (m C–H), 2000 (w, C–H), 1646 (s), 1399 (m, C=S), 798 (s, diimine)  $\text{cm}^{-1}$ .  $^{31}\text{P}\{\text{H}\}$  SS-NMR:  $\delta$  45, –145.  $^{13}\text{C}\{\text{H}\}$  SS-NMR:  $\delta$  203 (metal CO), 162 (C=S), 150–110 (aromatics), 60–15 (polymer), –6 (Si-Me).

**Spectroscopic Data for MPE-3.** IR in KBr: 2964 (m, C–H), 2921 (m, C–H), 1991 (w, metal CO), 1676 (s), 1399 (m, C=S), 796 (s, diimine ring)  $\text{cm}^{-1}$ .  $^{31}\text{P}\{\text{H}\}$  SS-NMR:  $\delta$  66, –145.  $^{13}\text{C}\{\text{H}\}$  SS-NMR:  $\delta$  207 (metal CO), 162 (C=S), 150–120 (aromatics), 55–20 (polymer), –6 (Si-Me).

**Spectroscopic Data for MPA-5.** IR in KBr: 2950 (s, C–H), 2935 (s, C–H), 1400 (s, C=S), 790 (vs, diimine)  $\text{cm}^{-1}$ .  $^{13}\text{C}\{\text{H}\}$  SS-NMR:  $\delta$  163 (C=S), 100–160 (aromatics), 60–20 (polymer), –6 (Si-Me).

**Spectroscopic Data for NPA-3.** IR in KBr: 2945 (s, C–H), 2932 (s, C–H), 1996 (w, metal CO), 1644 (s), 1398 (s, C=S), 795 (vs, diimine)  $\text{cm}^{-1}$ .  $^{31}\text{P}\{\text{H}\}$  SS-NMR:  $\delta$  60, –145.  $^{13}\text{C}\{\text{H}\}$  SS-NMR:  $\delta$  202 (metal CO), 162 (C=S), 135–110 (aromatics), 45 (C<sub>3</sub>), 24.3 (C<sub>2</sub>), 8.3 (C<sub>1</sub>), 50–15 (polymer), –6 (Si-Me).

**General Procedure for the Coupling of Complex 4 to the Composites by Direct Reaction with the Composites: Synthesis of MPA-4, MPE-4, and NPA-4.** A 75 mg amount of the complex 4 (0.07 mmol) was dissolved in 20 mL of  $\text{CH}_2\text{Cl}_2$  in a round-bottom flask along with 250 mg of BP-1 microparticles. Following the addition of BP-1, the reaction mixture was top stirred for an additional 3 h. The reaction was then stopped by removing the solvent from the particles, and ~20 mL of fresh  $\text{CH}_2\text{Cl}_2$  was added to wash the particles. The wash was achieved by top stirring the particles for 1 h and then removing the solvent, repeating the process three times. After the third wash the particles were collected and dried on a vacuum line.

**Spectroscopic Data for MPA-4.** IR in KBr: 2926 (m, C–H), 1986 (w, metal CO), 1634 (s, C=N), 1562 (m), 798(s)  $\text{cm}^{-1}$ .  $^{31}\text{P}\{\text{H}\}$  SS-NMR:  $\delta$  44, –145.  $^{13}\text{C}\{\text{H}\}$  SS-NMR:  $\delta$  203 (metal CO), 162 (C=N), 140–120 (aromatics), 40–20 (polymer), –6 (Si-Me).

**Spectroscopic Data for MPE-4.** IR in KBr: 2970 (m, C–H), 2920 (m, C–H), 1957 (w, metal CO), 1672 (s, C=N), 1584 (m), 798 (s, diimine)  $\text{cm}^{-1}$ .  $^{31}\text{P}\{\text{H}\}$  SS-NMR:  $\delta$  45, –145.  $^{13}\text{C}\{\text{H}\}$  SS-NMR:  $\delta$  163 (C=N), 140–120 (aromatics), 40–20 (polymer), –6 (Si-Me).

**Spectroscopic Data for NPA-4.** IR in KBr: 2926 (m, C–H), 1989 (w, metal CO), 1650 (s, C=N), 798 (s, diimine)  $\text{cm}^{-1}$ .  $^{31}\text{P}\{\text{H}\}$  SS-NMR:  $\delta$  59, –145.  $^{13}\text{C}\{\text{H}\}$  SS-NMR:  $\delta$  202 (metal CO), 151 (C=N), 135–110 (aromatics), 45 (C<sub>3</sub>), 24.3 (C<sub>2</sub>), 8.3 (C<sub>1</sub>), 50–15 (polymer), –6 (Si-Me).

## ■ ASSOCIATED CONTENT

### § Supporting Information

<sup>1</sup>H, <sup>13</sup>C, <sup>19</sup>F, and <sup>31</sup>P solution NMR for 4; <sup>13</sup>C CPMAS NMR spectra for MPA1–MPA4 and NPA1–NPA4. This material is available free of charge via the Internet at <http://pubs.acs.org>.

## ■ AUTHOR INFORMATION

### Corresponding Authors

\*E-mail: edward.rosenberg@mso.umt.edu.

\*E-mail: sandy.ross@umontana.edu.

### Notes

The authors declare no competing financial interest.

## ■ ACKNOWLEDGMENTS

We gratefully acknowledge the support of the National Science Foundation (CHE 1049569) and the National Institutes of

Health, Institute of General Medical Sciences (P20 GM103546), for support of this research. We also acknowledge OLiS Systems for measuring absorption spectra of the microparticles using their CLARiTY spectrometer. We also acknowledge Dr. Ayesha Sharmin for help with the lifetime measurements.

## ■ REFERENCES

- (1) Allen, J. J.; Rosenberg, E.; Johnston, E.; Hart, C. *ACS Appl. Mater. Interfaces* **2012**, *4*, 1573–1584.
- (2) Jal, P. *Talanta* **2002**, *62*, 1005–1028.
- (3) Allen, J.; Rosenberg, E.; Karakhanov, E.; Kardashev, S. V.; Maximov, A.; Zolotukhina, A. *Appl. Organomet. Chem.* **2011**, *25*, 245–254.
- (4) Jurss, J. W.; Concepcion, J. C.; Norris, M. R.; Templeton, J. L.; Meyer, T. J. *Inorg. Chem.* **2010**, *49*, 3980–3982.
- (5) Lu, X.; Manners, I.; Winnik, M. A. *Macromolecules* **2001**, *34*, 1917–1927.
- (6) Susha, A. S.; Javier, A. M.; Parak, W. J.; Rogach, A. L. *Colloids Surf. Physicochem. Eng. Asp.* **2006**, *281*, 40–43.
- (7) Sautet, P.; Delbecq, F. *Chem. Rev.* **2010**, *110*, 1788–1806.
- (8) Beatty, S. T.; Fischer, R. J.; Hagars, D. L.; Rosenberg, E. *Ind. Eng. Chem. Res.* **1999**, *38*, 4402–4408.
- (9) Rosenberg, E. In *Macromolecules Containing Metal and Metal-Like Elements*; J. Wiley & Sons: New York, 2005; Vol. 4, pp 51–78.
- (10) Rosenberg, E.; Hughes, M.; Neilsen, D.; Gobetto, R.; Viale, A.; Burton, S. D.; Ferel, J. *Ind. Eng. Chem. Res.* **2006**, *45*, 6538–6547.
- (11) (a) Rosenberg, E.; Pang, D. U.S. Patent No. 5,695,882, 1997. (b) Rosenberg, E.; Pang, D. U.S. Patent No. 5,997,748, 1999. (c) Rosenberg, E.; Fischer, R. U.S. Patent No. 6,576,590, 2003. (d) Rosenberg, E.; Fischer, R. U.S. Patent No. 7,008,601, 2006. (e) Rosenberg, E.; Miranda, P.; Wong, Y. O. U.S. Patent No. 8,343,446, 2012.
- (12) Soliman, E. M. *Anal. Lett.* **1997**, *30*, 1739.
- (13) Yoshitake, H.; Joiso, E.; Tatsumi, T.; Horie, H.; Yoshimura, H. *Chem. Lett.* **2004**, *33*, 872.
- (14) Kramer, J.; Driessens, W. L.; Koch, K. R.; Riedek, J. *Sep. Sci. Technol.* **2004**, *39*, 63.
- (15) Shiraishi, Y.; Nishimura, G.; Hirai, T.; Komasa, I. *Ind. Eng. Chem. Res.* **2002**, *41*, 5.
- (16) Anderson, C.; Rosenberg, E.; Hart, C. K.; Ratz, L.; Cao, Y. In *Proceedings of the 5th International Symposium on Hydrometallurgy*, Volume 1 Leaching and Purification; Young, C., Ed.; TMS: Warrendale, PA; 2003, p 393.
- (17) Cousinié, S.; Gressier, M.; Alphonse, P.; Menu, M.-J. *Chem. Mater.* **2007**, *19*, 6492–6503.
- (18) Fischer, R.; Pang, D.; Beatty, S. T.; Rosenberg, E. *Sep. Sci. Technol.* **1999**, *34*, 312.
- (19) Keles, M.; Keles, T.; Serindag, O.; Yasar, S.; Ozdemir, I. *Phosphorus Sulfur Silicon Relat. Elem.* **2010**, *185*, 165–170.
- (20) Menu, M. J.; Cousinié, S.; Mauline, L.; Gressier, M.; Kandibanda, S. R.; Datas, L.; Reber, C. *New J. Chem.* **2012**, *36*, 1355–1367.
- (21) Rosso-Vassic, M.; De Cola, L.; Zuilof, H. *J. Phys. Chem. C* **2009**, *113*, 2235–2240.
- (22) Sharmin, A.; Darlington, R. C.; Hardcastle, K. I.; Ravera, M.; Rosenberg, E.; Ross, J. B. A. *J. Organomet. Chem.* **2009**, *694*, 988–1000.
- (23) Sharmin, A.; Salassa, L.; Rosenberg, E.; Ross, J. B. A.; Abbott, A.; Black, L.; Terwilliger, M.; Brooks, R. *Inorg. Chem.* **2013**, *52* (19), 10835–10845.
- (24) Guo, X.; Li, L.; Castellano, H.; Szmacinski, H.; Lakowicz, J. R. *Anal. Biochem.* **1997**, *254*, 179.
- (25) Waddell, T. G.; Leyden, D. E.; DeBello, M. T. *J. Am. Chem. Soc.* **1981**, *103*, 5303–5307.
- (26) Borisov, O. V.; Coleman, D. M.; Oudsema, K. A.; Carter, R. O., III. *J. Anal. At. Spectrom.* **1997**, *12*, 239.

- (27) Lakowicz, J. R. *Principles of Fluorescence Spectroscopy*; Springer: New York, 2006.
- (28) Badea, M. G.; Brand, L. *Methods Enzymol.* **1979**, *61*, 378–425.
- (29) (a) Minazzo, A. S.; Darlington, R. C.; Ross, J. B. A. *Biophys. J.* **2009**, *96*, 681–692. (b) Johnson, M. L.; Frasier, S. G. In *Methods in Enzymology*, Vol. 117; Academic Press: New York, 1985; p 301.
- (30) Strouse, G. F.; Schoonover, J. R.; Duesing, R.; Boyde, S.; Jones, W. E.; Meyer, T. J. *Inorg. Chem.* **1995**, *34*, 473–487.
- (31) Carpino, L. A. *J. Am. Chem. Soc.* **1993**, *115*, 4397–4398.
- (32) Zhan, W.; Jiang, K.; Smith, M. D.; Bostic, H. E.; Best, M. D.; Auad, M. L.; Ruppel, J. V.; Kim, C.; Zhang, X. P. *Langmuir* **2010**, *26*, 15671–15679.
- (33) Szmacinski, H.; Terpetschnig, E.; Lakowicz, J. R. *Biophys. Chem.* **1996**, *62*, 109–120.
- (34) Hughes, M.; Wood, J.; Rosenberg, E. *Ind. Eng. Chem. Res.* **2008**, *47*, 6765–6774.
- (35) Shiriashi, Y.; Nishimura, G.; Hirai, T.; Komasawa, I. *Ind. Eng. Chem. Res.* **2002**, *41*, 5065–5070.
- (36) Fujita, E. *Coord. Chem. Rev.* **1999**, *185–186*, 373–38.